R4-C.1: Advanced Multispectral Computed Tomography Algorithms

I. PARTICIPANTS INVOLVED FROM JULY 1, 2019 TO JUNE 30, 2020

Faculty/Staff			
Name	**Title**	**Institution**	**Email**
Clem Karl	PI	BU	wckarl@bu.edu
David Castañón	Professor	BU	dac@bu.edu
Graduate, Undergraduate and REU Students			
Name	**Degree Pursued**	**Institution**	**Month/Year of Graduation**
Sandamali Devadithya	PhD, ECE	BU	6/2021
Usman Ghani	PhD, ECE	BU	6/2021

II. PROJECT DESCRIPTION

A. Project Overview

Explosives represent a continual threat to aviation security. New threats, resilient and adaptable adversaries, and demands for increased throughput continue to stress existing and planned security systems. New limited data geometries, novel sensing paradigms, and increased performance requirements have challenged traditional methods for Computerized Tomography (CT)-based explosives detection in security systems. Furthermore, CT-based systems are being developed and deployed for new missions, such as checkpoint carry-on screening and air cargo screening. Such systems use new sensing geometries with multi-spectral excitation.

In order to extract features that can identify explosives, CT systems are using dual-energy computed tomography (DECT) to estimate a small number of material-specific parameters at each image location and use them for material identification. Multispectral X-ray CT attempts to use the additional energy-dependent material information obtained by making multiple energy-selective measurements of attenuation. Metal and clutter in scenes cause artifacts that confound traditional methods. In addition, new sensing geometries are being explored. All these developments have meant that the application of conventional tomographic imaging approaches, largely coming from the medical domain, are highly suboptimal, and new approaches are required.

In this project, new methods for the formation of enhanced material parameter images from multi-energy CT data have been developed. The methods focus on increasing robustness to noise and artifacts that exist in images obtained by conventional means. The resulting algorithms include approaches for enhanced image quality and material identification. The improved algorithms lead to more accurate material and object identification, resulting in fewer false alarms, greater security, and reduced passenger inconvenience. These algorithms have been tested on simulated and real data.

B. *State of the Art and Technical Approach*

The majority of the work on multispectral X-ray CT focuses on DECT. Several DECT techniques have been suggested since the 1970s [1-3]. They are mostly targeted at medical applications and do not deal with the image artifact mitigation necessary for security applications [4-8]. Extensions of dual-energy techniques for security applications can be found in [8-9]. We overview the basic approach for DECT briefly below.

In DECT, X-ray transmission measurements of an image are collected using two excitations with different spectra. The observed normalized log-sinogram data in DECT sensing follows the nonlinear Beer-Lambert law [1,2,9]:

$$I_s(\ell) = -\ln\left(\frac{\int w_s(E) e^{-\int_\ell \mu(x,E)dx} dE}{\int w_s(E) dE}\right)$$

where $w_S(E)$ is the spectral weighting used in the measurement with spectrum s; $\mu(x,E)$ is the linear attenuation coefficient (LAC) of the material at spatial location x and energy E, and $I_S(\ell)$ is the measurement along ray-path ℓ for spectral weighting $w_S(E)$. Examples of LAC curves and spectral weighting functions are shown in Figure 1.

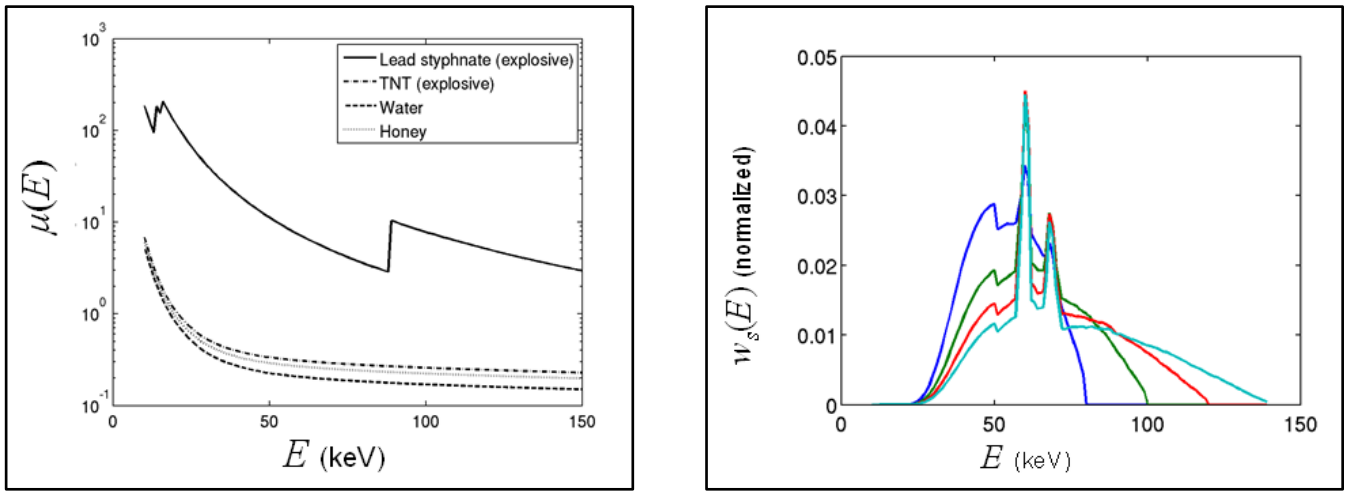

Figure 1: (left) The LAC curves of a few example materials and (right) examples of spectral weighting functions (normalized to unit sum).

The characteristics of the material at spatial location x are captured through the energy dependent function. Typically, this function is approximated as a linear combination of a few basis functions [1, 8]. A common choice of basis functions in DECT are the photoelectric absorption and Compton scatter cross-section functions. The LAC representation in the photo-Compton model is given by:

$$\mu(x,E) = a_p(x) f_p(E) + a_c(x) f_c(E)$$

where $f_p(E), f_c(E)$ are the photoelectric and Compton energy-dependent basis functions; and $a_p(x)$, $a_c(x)$, are the corresponding material-dependent coefficients at each spatial location x. The goal is to separate materials on the basis of their coefficient values.

In many DECT methods, the goal is to reconstruct the coefficient images $a_p(x)$ and $a_c(x)$, given the dual-energy tomographic projection measurements $I_1(\ell)$, $I_2(\ell)$. Since the problem is nonlinear and high dimensional, a

well-known solution approach is to separate it into two decoupled subproblems [1]. In the first subproblem, a nonlinear set of equations is solved at each detector, to obtain the basis coefficient sinograms $A_p(\ell)$, $A_c(\ell)$, defined as:

$$A_p(l) = \int_{\ell} a_p(x)\,dx \text{ and } A_c(l) = \int_{\ell} a_c(x)\,dx.$$

The second subproblem is tomographic reconstruction of the basis coefficient images $a_p(x)$ and $a_c(x)$ from these sinograms. This reconstruction step is usually accomplished by applying filtered back projection (FBP) or iterative reconstruction methods to each sinogram individually; therefore, mutual structure information is not used.

An early focus of this work was on developing reconstruction algorithms that simultaneously formed basis coefficient images and exploited mutual structure information in each sinogram. We called this method structure-preserving dual-energy (SPDE), which was documented in our past publications [10-12].

The general formulation of our SPDE method in vector form is given by the following:

$$\min_{(a_p \geq 0, a_c \geq 0, s)} \| A_p - Ta_p \|_{W_z}^2 + \| A_c - Ta_c \|_{W_z}^2 + \lambda_1 \| Da_p \|_{W_{ps}}^2 + \lambda_2 \| Da_c \|_{W_{cs}}^2 + \lambda_3 \| a_p \|_2^2 + \lambda_4 \| a_c \|_2^2 + \lambda_5 \| Ds \|_2^2 + \lambda_6 \| s \|_2^2$$

where s is a common mutual boundary field; T is the tomographic projection operator; D is a derivative operator; W_z is a data weighting matrix; W_{ps} and W_{cs} are weighting matrices derived from s; and λ_k are nonnegative regularization parameters.

Another major result in our previous work was the development of a joint segmentation/recognition approach for direct estimation of material labels from dual-energy labels. In typical explosive detection systems [10-12], segmentation of reconstructed images is used to identify volumes of interest, from which features are extracted to classify the volume. In our approach, we formulate a combined segmentation/classification optimization problem for dual-energy systems. We extended the previous multi-energy formulation to direct estimation of material labels but combined a dual-energy learned appearance model with a Markov random field material model. In the dual-energy case this formulation becomes:

$$\min_{l_1, l_2, \ldots, l_N} \left\{ \sum_x v_x [-\ln\left(p(\mu_x^L, \mu_x^H | l_x)\right)] + \lambda g_{MRF}(l_1, l_2, \ldots, l_N, s) \right\}$$
$$\text{subject to } l_x \in \{1, 2, \ldots, M\}$$

where μ_j^L, μ_j^H are the formed effective attenuation images obtained from measurements with two different (high and low) spectral weightings at voxel x; l_x is the material label at voxel x; $p(\mu_j^L, \mu_j^H \mid l_x)$ is the learned appearance model for material label l_x at voxel x; v_x are data weights, which down-weight data points in the vicinity of metal; λ is a nonnegative regularization parameter; and $g_{MRF}(l_1, l_2, \ldots, l_N, s)$ is a Markov random field smoothing term, which is based on an estimate of the image boundary field s. This MRF model captures local coherence of material labels and takes into account an estimate of object boundaries to further ensure label homogeneity within an object.

The resulting optimization problem is a nonconvex, discrete label problem, which is generally challenging to solve. To accomplish this optimization, we developed an efficient graph-cut method. Such graph-cut methods [13] have been popular in computer vision and discrete optimization literature but have not been used in this domain. These methods map the original optimization problem to an equivalent graph flow problem, and a minimal cut of this graph provides the optimal solution when there are only two labels. In our experiments, there are multiple labels, so we use a rotation method to obtain a solution. We call this voxel-

based method "learning-based object identification and segmentation," or LOIS. Our algorithm development and initial results were documented in [10-,11].

In our recent work, we extended this approach to learn spatially correlated models of the dual-energy reconstructions for different materials. Using sample reconstructions that include regions with known materials, we learn the conditional probability density of the low and high attenuation images over a neighborhood patch that includes *k* pixels, as:

$$p(\mu_{1,n}^{L}, \ldots, \mu_{k,n}^{L}, \mu_{1,n}^{H}, \ldots, \mu_{k,n}^{H} | \ell_n)$$

where $\mu_{j,n}^{L}$, $\mu_{j,n}^{H}$ refers to the reconstructed low and high attenuation for pixel number *k* in patch at location *n*.

In our work, we use patches consisting of 2×2 pixels to better capture the special energy dependence. We then optimize the following energy function over the labels and patches:

$$\min_{\{\ell_n, n=1,\ldots,NN\}} \sum_{n=1}^{NN} p(\mu_{1,n}^{L}, \ldots, \mu_{k,n}^{L}, \mu_{1,n}^{H}, \ldots, \mu_{k,n}^{H} | \ell_n) + \lambda \sum_{n=1}^{NN} \sum_{n \in \mathcal{N}(n)} \phi(\ell_n, \ell_j)$$

where *NN* is the number of patches; ℓ_n is the label of patch *n*; and $\phi(\ell_n, \ell_j)$ is 0 if $\ell_n = \ell_j$, 1 otherwise. The resulting discrete optimization problem is solved by a multi-label graph-cut algorithm [22], leading to fast assignment of material labels to patches. The development of the patch-based version of the LOIS algorithm was presented in our paper [14] and the thesis [15].

The LOIS approach described above for the joint segmentation/classification of materials requires the formation of CT images. As part of our research under this task, we have also developed approaches that can directly estimate discrete labels associated with spatial regions from single-energy or dual-energy sinograms. This bypasses conventional CT image formation and results in discrete tomography formulations. In our work, we examined the difficult general problem of inverting tomographic data where the scene is constrained to be discrete valued using a variational approach. Our original problem is defined as:

$$\underset{x \in \{\text{Disc Amp}\}}{\operatorname{argmin}} J_{data}(x) + \lambda J_{prior}(x) = \underset{x \in \{\text{Disc Amp}\}}{\operatorname{argmin}} J_{data}(x) + \lambda \|\mathrm{D}x\|_1^1$$

where *x* is the desired, unknown, discrete-valued quantity of interest; $J_{data}(x)$ is a data penalty (e.g., negative log-likelihood) that projects how the label field would generate sinograms that match the observed data; and $\|\mathrm{D}x\|_1^1$ is a total-variation edge-preserving dissimilarity penalty on the reconstructed label field.

The above formulation is a combinatorial formulation: each voxel must be labeled with one of a finite number of material labels (which includes background). As such, this is no longer a convex optimization problem of the type solved by iterative CT algorithms. Furthermore, the data fidelity term now involves matching the sinogram data, rather than matching the learned appearance model in the image space. The tomographic relationship between sinograms and the underlying properties of the label images does not permit the direct application of fast combinatorial algorithms, such as graph cuts, to solve the discrete problem.

Our early work on discrete tomography is documented in [16-17]. Our approach in that work was focused on extensions of graph-cut algorithms that would be applicable to discrete tomography, either through sequential linearization or through the use of decomposition techniques. We ended up pursuing a different algorithmic approach, developing a new variable splitting approach based on the alternating direction method of multipliers (ADMM) from convex optimization theory. ADMM is designed to solve convex optimization problems involving two blocks of variables by splitting the overall hard optimization into a sequence of simpler optimizations [18]. The ADMM algorithm is used for convex optimization with continuous variables, and our discrete optimization framework is notably nonconvex.

The ADMM-based algorithm that we developed, which we term TOMO-SPL, provides an efficient, inherently discrete solution; however, using a particular variable splitting:

$$x^{k+1} = \arg\min_{x \in \Re^n} J_{data}(x) + \frac{\rho}{2}\left\| x - z^k - u^k / \rho \right\|_2^2$$
$$z^{k+1} = \arg\min_{z \in \{\text{Disc Amp}\}} \lambda J_{prior}(z) + \frac{\rho}{2}\left\| x^{k+1} - z - u^k / \rho \right\|_2^2$$
$$u^{k+1} = u^k - \tau\rho\left(x^{k+1} - z^{k+1}\right)$$

Specifically, we reconstruct a continuous approximation to the discrete label field in the form of x, and we then solve for the best label z to assign to that discrete field that is close to x. Our particular splitting thus breaks down (in a joint iterative optimization) a field reconstruction step similar to CT iterative reconstruction, together with a joint segmentation/label step; the former step is done using standard iterative CT techniques, whereas the latter step can be performed efficiently using graph-cut techniques. This work was documented in our papers [19-21].

Another result from Year 4 that integrates learning into reconstruction is the development of a new algorithm to reduce metal artifacts in CT images when data is acquired using a single source spectrum. This is a major problem in both medical and security CT [4-5, 7]. Such metal artifacts arise from many effects, including beam hardening. With a single energy spectrum, one cannot use basis decomposition techniques to correct these artifacts.

Our algorithm is a hybrid approach that corrects the sinogram vector followed by an iterative reconstruction. Many prior sinogram correction algorithms [22–24] identify projection measurements that travel through areas with significant metal content and remove those projections, interpolating their values for use in subsequent reconstruction. In contrast, our algorithm retains the information of random subsets of these metal-affected projection measurements, and uses an average procedure to construct a modified sinogram. To reduce the secondary artifacts created by this interpolation, we apply an iterative reconstruction in which the solution is regularized using a sparsifying transform [25]. The basis functions used in the sparsifying transform are learned from reconstructed imagery, enforcing the natural structure that appears in CT reconstructions. Our experiments indicate that our algorithm reduces the extent of metal artifacts significantly, and it enables accurate recovery of structures in proximity to metal. These results are documented in our publication [26].

In the above discussion, we primarily focused on dual-energy CT systems. The emergence of new threat materials and variations in manufacturing processes have introduced new challenges for separating materials of interest using dual-energy spectra. There has also been an increase in new measurement technologies for extracting additional signatures that would enhance the capability for identifying materials, including commercial photon-counting detectors to facilitate multi-spectral CT and new measurement technologies (e.g., X-ray diffraction imaging and phase contrast imaging). Furthermore, new features are being proposed for dual-energy systems, either in terms of basis materials or in terms of electron density or effective atomic number [1,8,27].

Given these developments, it is important to understand the limits in performance of potential designs for new systems that include changes in architecture, processing, measurement technology, and extracted features. To that end, we developed an approach based on information theory metrics that provides bounds on the explosives detection performance of alternative system architectures with different feature extraction approaches.

A drawback of using information theory is that computing the measures requires knowledge of the underlying probability distributions of the features for different materials. Furthermore, exact computation

can only be conducted for small classes of distributions such as Gaussian, Poisson, or exponential models. An alternative approach uses machine learning and nonparametric techniques, such as kernel density estimation, to estimate the underlying probability distributions of the different material classes from sample values. Unfortunately, most of these nonparametric techniques result in densities for which the relevant information theory divergence measures cannot be computed in closed form. This requires Monte Carlo techniques, a process that can be slow and require many samples when the feature values are multidimensional.

In our work in Year 4, we adapted novel techniques in nonparametric statistics for estimating information-theoretic measures of explosives detection performance directly using graph techniques, avoiding the need to learn distributions. Our algorithms are graph-based estimators based on minimal spanning trees that compute an approximation to a particular *f*-divergence measure. This *f*-divergence can estimate bounds on the Fisher information as well as the Bayes error in binary classification [28]. Unlike many other divergence measures, this *f*-divergence can be estimated directly from data samples without generating estimates of the underlying distributions. In our paper [29], we describe a framework for performance estimation for novel threat detection systems using these performance bounds. We illustrate the framework by computing bounds on the Bayes error for a class of multi-spectral X-ray CT systems using photon-counting detectors with different energy quantization bins.

The use of photon-counting detectors, or with additional illumination spectra beyond two, raises the possibility of extracting more than two features for summarizing material properties. Previous work [1, 8, 27] has established that two features (such as photoelectric and Compton coefficients) are usually sufficient to represent the linear attenuation properties of materials with an effective atomic number below 14. However, this representation is inaccurate for many explosive materials, such as Baratol or lead styphnate, which have component elements with K-edges in the relevant energy range of the CT instruments (usually 30–120 keV). In Year 5, we explored the utility of additional basis representations when photon-counting detectors are used. We developed CT algorithms that can reconstruct the coefficients of the different materials in an image from multi-energy projection sinograms. These algorithms are extensions of the dual-energy approach in [1, 8, 17], using enhanced sparse optimization techniques and statistical methods. The idea is to select basis representations that capture the variability of the LACs in Figure 1 accurately.

Some of the potential basis representations that we explored are based on machine learning features. Given a database of materials with LACs, one can find basis functions using principal component analysis, and select the basis corresponding to the three to five largest principal directions, which typically capture most of the variability among the LACs of the different materials. If we separate the materials into explosives and non-explosives, we can choose basis functions with techniques from discriminant analysis, which can capture the primary differences between the explosive class and the non-explosive class. In particular, we explored the use of the sequential linear discriminant analysis basis suggested in [12]. As a final set of basis functions, we explored extensions of physical bases such as photoelectric and Compton, adding the linear attenuation functions of materials with K-edges in the 30–120 keV region. While this last set of bases may have more functions than spectra used for sinogram measurements, we used a sparse decomposition where the measured photon counts for each spectrum *k,* denoted by b^k and converted to log scale, are decomposed at each detector into sparse coefficients α for the basis using the following optimization:

$$\min_{\alpha} \sum_{k} || \ln(\int_{e \in S_k} w_k(e) e^{-B^T(e)\alpha} de) + \frac{\ln(b^k)}{\ln(I^k)} ||_2^2 + \lambda ||\alpha||_1$$

The resulting decomposition at each detector can be used to construct coefficient images, which provide the needed signals for explosives detection. Our results [15,30] established that this last set of basis functions

could be used to obtain accurate reconstructions of materials with high effective atomic numbers, provided their attenuation was small enough to allow for X-ray penetration.

The main focus of our Year 6 work was on transitioning selected multispectral algorithms developed in earlier years for use in commercial CT systems for Department of Homeland Security (DHS) missions. In particular, we focused on developing algorithms for a dual-energy air cargo CT inspection system developed by our industrial partner, Astrophysics Inc. The challenge was to develop reconstruction and feature extraction approaches that achieve enhanced resolution, reduce artifacts, and increase the accuracy of object recognition, as well as achieving real-time computation objectives so that the resulting algorithms become part of a fielded prototype system.

To enhance the resolution of the resulting dual-energy system, we developed a major improvement for the joint inversion approach, SPDE, that we had developed earlier in our program. In our paper [31], we improved on this approach by developing an edge-preserving total variation (EPTV) regularization algorithm that provides sharp boundary definition, even in regions where the materials are hard to observe. The main idea in this technique is to identify edges from an initial reconstruction, typically from the high energy image. We then define voxel-dependent regularization weights based on the magnitude of the gradient of the image. In two dimensions, these weights are defined as:

$$\mathbf{w}_v = \exp(-(|\mathbf{D}_v\mathbf{x}_{high}|)/\sigma) \quad \mathbf{w}_h = \exp(-(|\mathbf{D}_h\mathbf{x}_{high}|)/\sigma)$$

where D_v and D_h are the vertical and horizontal directional gradients, and σ is a scale parameter. Using these edge-dependent weights, the reconstructed photoelectric and Compton images are generated using a weighted total variation iterative reconstruction technique, as the solution of:

$$\hat{\mathbf{x}}_c = \underset{\mathbf{x}_c \geq 0}{\operatorname{argmin}} \frac{1}{2}||\mathbf{y}_c - \mathbf{A}\mathbf{x}_c||_2^2 + \tau_c||\mathbf{W}_h\mathbf{D}_h\mathbf{x}_c||_1 + \tau_c||\mathbf{W}_v\mathbf{D}_v\mathbf{x}_c||_1$$

$$\hat{\mathbf{x}}_p = \underset{\mathbf{x}_p \geq 0}{\operatorname{argmin}} \frac{1}{2}||\mathbf{y}_p - \mathbf{A}\mathbf{x}_p||_{\mathbf{W}_{yp}}^2 + \tau_p||\mathbf{W}_h\mathbf{D}_h\mathbf{x}_p||_1 + \tau_p||\mathbf{W}_v\mathbf{D}_v\mathbf{x}_p||_1$$

where the matrices W_v and W_h are defined by the weight coefficients derived from the initial reconstruction.

In Year 6 and 7, we continued our metal artifact reduction (MAR) work using deep neural networks, which we started in Year 5. One of the limitations of the MAR approach we developed in [14,15] was the large computation requirements. We have developed deep learning methods for artifact reduction in X-ray tomographic images. Many groups are applying conventional methods from computer vision to post-process images and are attempting to improve them. In contrast, we have focused on removing artifacts directly from tomographic projection data prior to image formation. The advantage of our approach is that it fits well into conventional data processing flows. In particular, once trained, applying a convolutional network to sinogram data can be very fast if it's followed by conventional FBP reconstruction. Thus, our method can plug into existing vendor processing workflows with little alteration. Further, it is much faster during evaluation than computationally intensive iterative methods.

C. Major Contributions

One of the major results of our work in Years 1 and 2 was the development of the SPDE reconstruction framework that generates a unified, joint estimate of the coefficient images for dual-energy CT. We implemented a 2D version of this frame and demonstrated results in reducing the artifacts in dual-energy photoelectric and Compton imagery on two representative slices using data generated for ALERT under Task Order 3 (TO3) [32].

In previous annual reports, we have detailed results of our experiments with this algorithm, documented in [11, 32]. Figure 2 shows results obtained from 95 kVp and 130 kVp data obtained from the Imatron C300 CT scanner under TO3. The top row shows the results of conventional reconstructions of the photoelectric and Compton coefficients. The presence of metal causes severe streaking in the photoelectric image and causes shading and intensity variation in homogeneous regions of the Compton image. Such light and dark streaking can lead to object splitting in subsequent segmentation and label tasks of an automatic target recognition, thus compromising threat identification. In contrast, the bottom row shows our SPDE method. The reduction of streaking artifacts is readily apparent, as is the improved uniformity of homogeneous object regions.

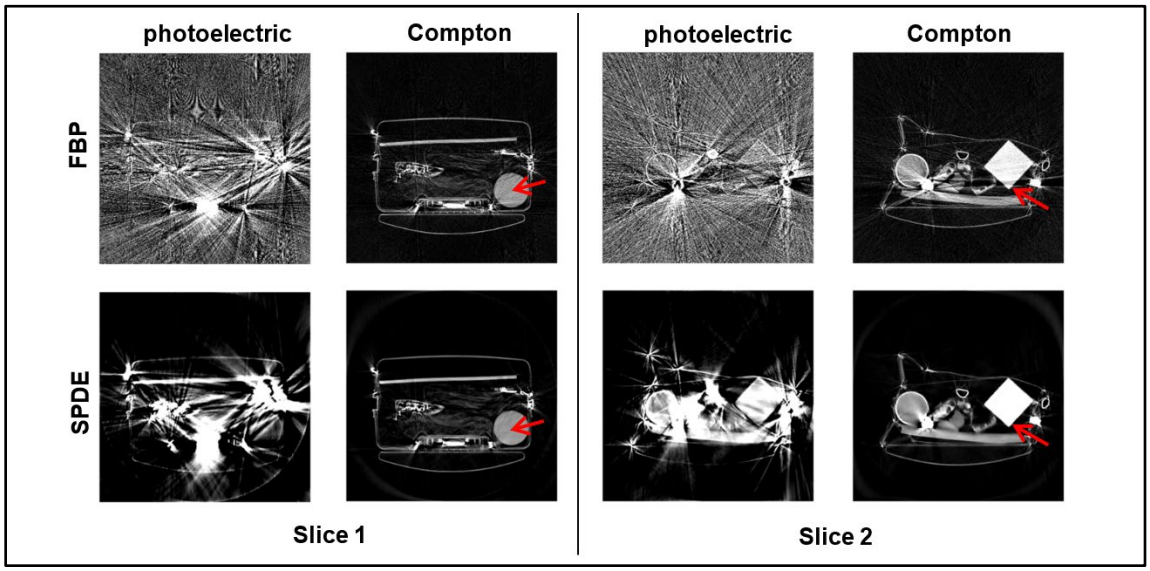

Figure 2: Two example slices from the Imatron data set for TO3; (top) conventional FBP-based photoelectric and Compton reconstructions based on decoupled processing. Severe streaking and shading due to metal are evident; (bottom) new SPDE reconstructions. Reduction of streaking and improved uniformity of object regions are demonstrated.

Another major result of our efforts from Years 2 and 3 was the learning-based joint segmentation and classification algorithm, LOIS, documented in [10-12]. In Year 4, these results were extended to a patch-based formulation to account for spatial correlations in voxel values [14]. To illustrate the improvements of the patch-based LOIS over the voxel-based LOIS algorithm, we tested both algorithms on some of the dual-energy reconstructions obtained from the TO3 dataset [32]. This data was collected on the Imatron scanner with two different peak voltages, 135 kV and 95 kV. Based on multiple images, we trained both a single-pixel appearance model and a 2×2 patch-based appearance model. The improvements are documented in [14].

Another result in Year 4 was the development and implementation of the ADMM-based framework for discrete tomography that we term TOMO-SPL [19-21]. The variable splitting used in this framework breaks the original problem into subproblems that allow for the use of very efficient graph-cut methods, but more importantly, the overall solution method is very robust to data imperfections, as we illustrate next. Figure 3 demonstrates the results of using our discrete tomography algorithm on an extremely sparse angle tomography problem with only eight projections, a very limited-angle problem. The phantom is binary valued. The results show that TOMO-SPL has enhanced accuracy over the alternatives based on gray-scale reconstruction followed by discretization.

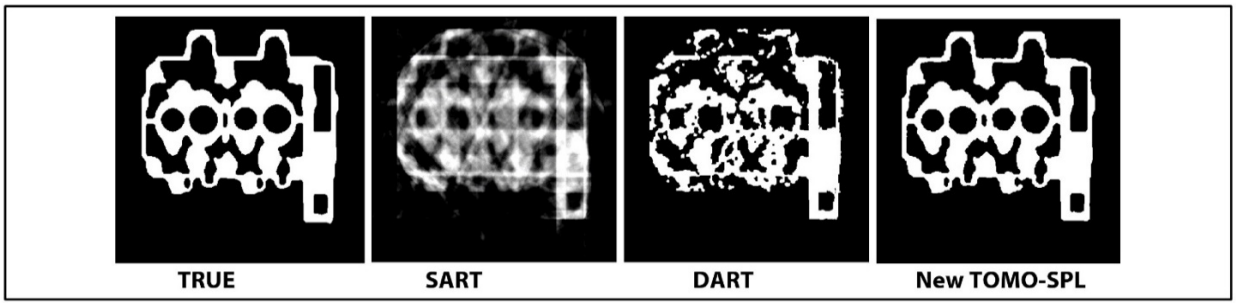

Figure 3: Comparison of results with only eight projections: True is the true field; SART is a conventional thresholded reconstruction based on the SART method; DART is the popular "discrete algebraic reconstruction tomography" method; and TOMO-SPL is our new method. Our new method produces nearly perfect reconstructions even from extremely limited data.

Note that TOMO-SPL preserves the connectivity between regions, prevents splits, suppresses noise, and maintains boundaries. These characteristics would prove valuable for use in new scanner geometries that use limited-angle sensing for speed, size, or power reasons.

Other results in Year 4 included the new approach for MAR documented in [15,26]. The approach combines aspects from dictionary learning together with random sampling to provide enhanced reconstructions in regions with significant metal presence. We tested the algorithms both on simulated data, as well as data obtained from the Imatron scanner with significant metal presence. A key aspect of our algorithm is that it tries to preserve the information in projections that pass through metal regions. In simulated experiments, the average reconstructed attenuation coefficient in regions enclosed by metal was far more accurate than in competing algorithms in the literature.

Another result in Year 4 was our work on performance bounds for detection performance of CT systems using nonparametric statistics. The key concept in our results, as explained in [28,29], is to simulate representative measurements from different materials and reconstruct features as points in n-dimensional space. By computing a minimum spanning tree using Euclidean distances for those points, one computes a statistic—namely the fraction of arcs in the minimum spanning tree that connect a point in one class (explosives) to a point in the other class (non-explosives). This statistic converges to an f-divergence that can be related to upper and lower bounds on the probability of error in detection.

To evaluate our techniques, we constructed a database of 320 materials, with 124 explosives and 196 non-explosives. For each of these materials, we obtained LAC information from National Institute of Standards and Technology models and used this to generate representative LACs as a function of X-ray energy. We then simulated measurements generated by photon-counting detectors with counts aggregated to varying numbers. As features, we reconstructed the average LACs in each detector energy bin. We also simulated measurements for a dual-energy system using photoelectric and Compton basis reconstructions. Our results are reported in the paper [29].

In Year 5 and continuing into Year 6 and 7, we developed deep learning methods for artifact reduction in X-ray tomographic images. Our techniques are focused on removing artifacts directly from tomographic projection data prior to image formation. Once trained, applying a convolutional network to sinogram data can be very fast, making our method suitable for transition, as it is much faster than alternative MAR techniques.

An overview of the approach is shown in Figure 4. We train a fully convolutional network to effectively remove metal artifacts in stream of commerce sinograms, conventionally reconstruct the output, and then

add the metal back in. By using modern conventional networks together with generalized adversarial learning [33], we can apply the network to the entire sinogram and not be limited to small patch-based processing, as some existing methods are. Since obtaining matched pairs of real sinograms for training is challenging, instead, we generate synthetic pairs by coupling a physically accurate X-ray simulator with a bag generator and then augment this synthetic data with modest real measurements via transfer learning.

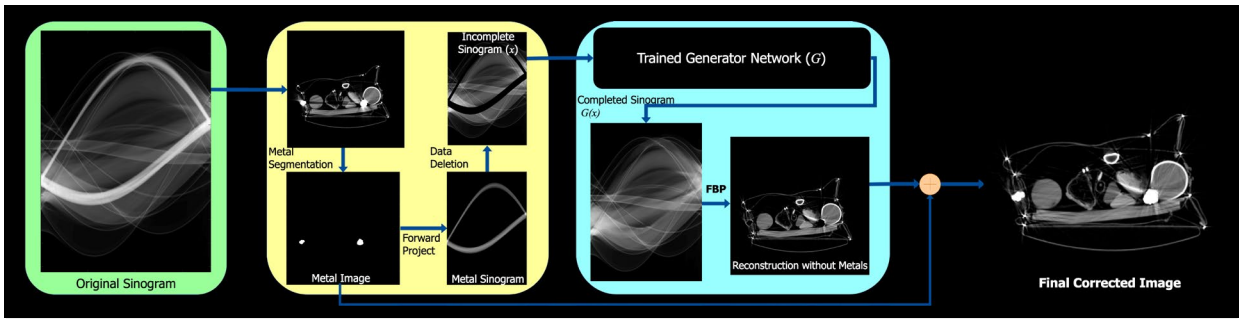

Figure 4: Overview of deep network MAR process.

We show some results in Figures 5 and 6. We compare our novel conditional generative adversarial network (CGAN) method with traditional linear interpolation and weighted nearest neighbor MAR methods. These preliminary results focus only on suppression of artifacts from large metal objects; they have not been optimized. Further results can be found in our papers [34-38]. In Year 6, we further developed these initial results scaling up the training as well as testing of the method. The method was also extended to sparse angle and low-dose tomography problems, where sinogram angular coverage is limited.

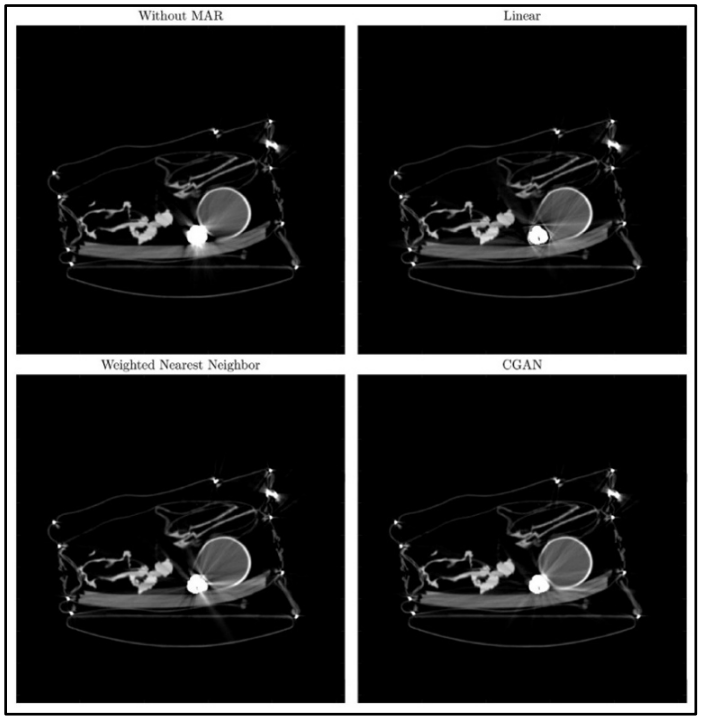

Figure 5: Comparison of MAR techniques for two slices of different suitcases with metal: (top left) original reconstruction; (top right) linear interpolation; (bottom left) weighted nearest neighbor algorithm; and (bottom right) reconstruction using our convolutional network MAR.

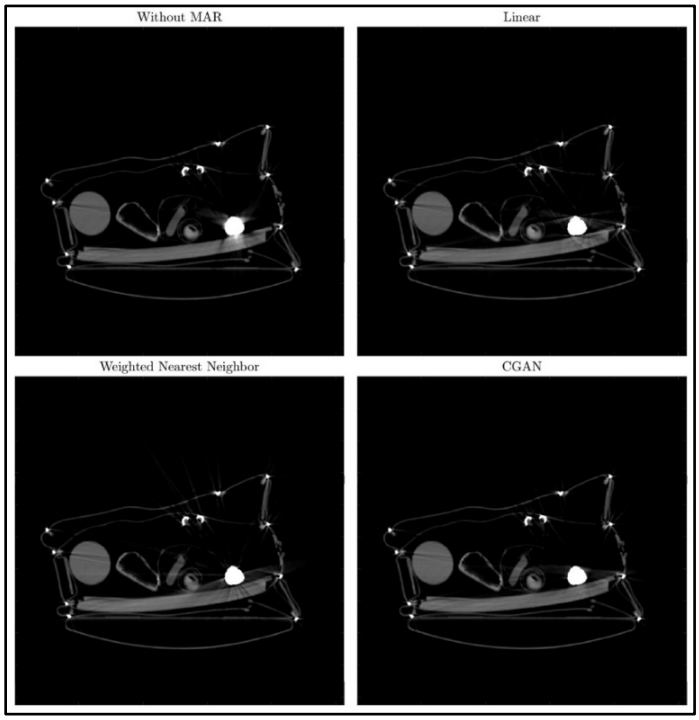

Figure 6: Comparison of MAR techniques for two slices of different suitcases with metal: (top left) original weighted nearest neighbor algorithm; (top right) linear interpolation; (bottom left) weighted nearest neighbor algorithm; and (bottom right) reconstruction using our convolutional network MAR.

In Year 5, we developed new multispectral CT algorithms that use more than two spectra and use a new class of basis functions that can accurately represent energy-dependent X-ray transmission characteristics in few dimensions. Current approaches for dual-energy decomposition use basis functions such as photoelectric and Compton cross-sections that have a continuous dependence on energy. However, many materials of interest—including explosives such as Baratol, where the LAC has discontinuities in energy due to the presence of atoms that include K-edges in the relevant energy region of the excitation—are used as contrast agents in medical imaging [39–41] precisely because their X-ray attenuation increases at specific energies that can be identified using multispectral CT imaging. However, medical imaging approaches for multispectral CT have been limited to direct imaging of each spectral signature separately, avoiding basis decompositions.

One of our main contributions is the development of a new class of basis functions that can represent the LACs of complex materials that include atoms with K-edges in the region of interest. Figure 7 illustrates the LAC of Baratol versus energy, with a discontinuity in energy arising because of the K-edge of barium around 38 keV. As the figure indicates, the LAC of Baratol is poorly approximated using a photoelectric-Compton basis, and imaging with dual-energy systems in this basis leads to Baratol being classified as iron.

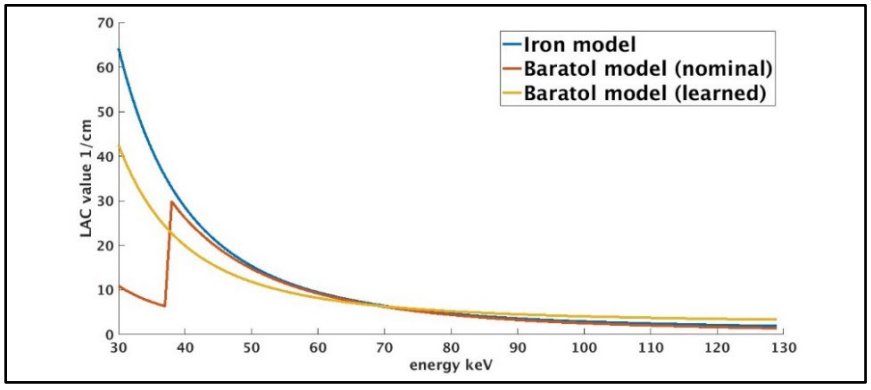

Figure 7: LAC of Baratol versus energy (red); best approximation using photoelectric and Compton basis (orange); and material that is confused with Baratol when using dual-energy CT (blue).

To address this problem, we investigated several approaches at modifying the set of basis functions used for multispectral imaging systems. Specifically, we introduced a new basis transform, termed SPECK, which is a short form for "sparse photoelectric, Compton, and K-edge basis." The first two basis functions in the transform are the photoelectric and Compton basis functions. To these two functions, we added the LAC functions of the atoms that have K-edges in the energy range 30–130 keV. Note that these other basis functions are linearly independent from the first two bases and each other because they have discontinuities at different energy values. However, the number of basis functions K can be larger than the number of spectral measurements in each detector, so we developed a different approach to estimate the decomposed measurements. Specifically, we proposed sparse regression techniques, where the decomposed measurements $A_L^1,\ldots, A_L^K$ are obtained for each detector by solving:

$$[A_L^1,\ldots,A_L^K] = \arg\min_{\underline{A}\geq 0} \sum_{i=1}^{I} (c_L^i - g^i(\underline{A}))^2 + \lambda \sum_{i=1}^{K} |A^i|$$

for a parameter λ that controls the desired level of sparsity in the coefficient vector. The details of this algorithm can be found in [15, 30].

We also developed a multispectral CT reconstruction algorithm that takes the estimated coefficient sinograms from the previous equation and constructs coefficient images in the volume of interest. We implemented a joint reconstruction and recognition algorithm and tested it on simulated data from a multispectral system photon-counting detectors with ten energy bins in the energy range of 30–130 keV. The reconstructed coefficient images were used to recognize the type of material in each region. We compared the performance of the multispectral algorithms using the SPECK basis decomposition, the photoelectric-Compton basis decomposition, reconstruction of the average LAC in each energy bin, and a data-driven basis derived from principal component analysis of a large set of materials. The results in Table 1 show that the multispectral CT with the SPECK basis significantly outperformed the alternatives in material recognition.

Algorithm	Region Classification Accuracy
SPECK coefficients	86.7%
PEC coefficients	75.0%
Direct LAC reconstruction	65.6%
PCA (6 coefficients)	61.6%

Table 1: Material recognition performance for multispectral CT experiments using different basis decompositions.

We also performed a set of experiments to recognize whether a material was an explosive or not using the same basis functions. In these experiments, we trained a random forest classifier on a set of 80 training images containing multiple materials, and then we tested the classification performance on a set of 20 test images. We ran the experiments with different regions of responsibility around each material, where larger regions (10%) indicated a range of 10% variability from the nominal LAC of each material in the test data. The resulting performance is shown in Table 2. The use of the SPECK basis improved explosives detection performance. Furthermore, the performance of the detection algorithms using the SPECK transform exhibited little degradation with increased region of responsibility, unlike the results for other algorithms.

Algorithm	Accuracy (0% variability)	Accuracy (5% variability)	Accuracy (10% variability)
Pho/Compton	94.1%	90.055	89.5%
PCA-6	04.8%	86.0%	83.0%
SPECK	99.4%	96.0%	96.0%
Direct Recon	94.1%	88.8%	85.0%

Table 2: Explosives detection performance for multispectral CT experiments using different basis decompositions.

The final set of results in Year 5 was the development of a novel approach toward joint CT reconstruction, segmentation, and identification. This can be viewed as a significant generalization of our work on discrete CT discussed earlier. In discrete CT, the underlying volume being imaged is composed of regions with constant LACs, and the imaging model is assumed to be linear. In our model, the underlying volume is composed of regions with constant material types, where the LACs of material types can vary within each region and will be energy dependent, as is the case when using Bremsstrahlung X-ray sources. As such, the corresponding imaging model is nonlinear, as discussed earlier.

The resulting algorithm, termed JRIDE (for "joint reconstruction and identification"), is illustrated in Figure 8. The basis decomposition sinograms are inputs to the algorithm. JRIDE reconstructs basis coefficient images as well as the material labels for the different regions in the image.

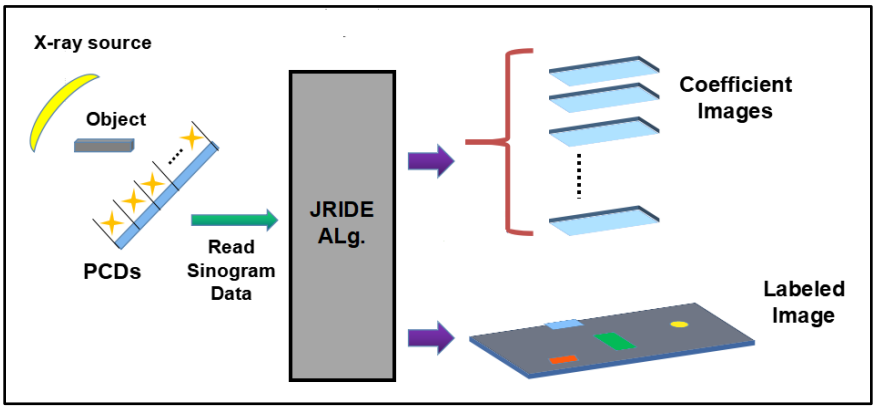

Figure 8: Structure of JRIDE algorithm.

The details of the JRIDE algorithm can be found in [15,42]. JRIDE performs a maximum a posteriori estimate of both the coefficient images as well as the underlying region labels. As such, the problem is posed as a joint optimization over region labels *Z* and coefficient images *W*:

$$(W^*, Z^*)(V) \in \arg\min_{W,Z} \frac{1}{2} \sum_{j=1}^{N_v d_c} (\hat{\mathbf{v}}_j - (M_j W)^T)^T \Sigma_j^{-1} (\hat{\mathbf{v}}_j - (M_j W)^T) + \beta \sum_{i=1}^{N_p} \sum_{i' \in \mathcal{N}(i)} ||\mathbf{w}(i) - \mathbf{w}(i')||^2$$

$$+ \sum_{i=1}^{N_p} \frac{1}{2} [(\mathbf{w}(i) - \mathbf{g}_{\ell(i)})^T \Gamma_{\ell(i)}^{-1} (\mathbf{w}(i) - \mathbf{g}_{\ell(i)}) + \log(\det(\Gamma_{\ell(i)})] + \gamma \sum_{i=1}^{N_p} \sum_{i' \in \mathcal{N}(i)} 1_{\ell(i) \neq \ell(i')}$$

The minimization is broken into overlapping minimizations, where given the coefficient image reconstructions *W*, one finds the best segmentation and material labels for regions *Z* (a discrete optimization) using an efficient multilabel graph cut algorithm [13]. Subsequently, given the region segmentation and

material labels, the coefficient images can be reconstructed as a continuous optimization problem where the coefficient reconstructions in each segmented region should be consistent with the region's material label.

Our JRIDE algorithm is similar in intent to a recent algorithm proposed for medical imaging in [43], named JE-MAP. The major differences between JRIDE and JE-MAP are twofold: first, JRIDE is based on a rigorous probabilistic maximum a posteriori framework; and second, JRIDE uses an efficient discrete optimization algorithm that is orders of magnitude faster than the corresponding algorithm used in JE-MAP. We evaluated our algorithm, JE-MAP, and an algorithm based on the conventional reconstruction, then we segmented and sequence classified the algorithms using a set of phantoms with 54 different materials present. The results are shown in Table 3. The JRIDE algorithm outperforms JE-MAP significantly, indicating the advantages of using a correct and rigorous probabilistic framework for the joint reconstruction and material identification problem. The results also indicate that there is significant improvement in material identification performance when material properties are used in an integrated manner with reconstruction, as indicated by the difference in performance between the sequential and JRIDE algorithms.

Algorithm	Region Classification Accuracy, No K-Edge Materials	Region Classification Accuracy, All Materials
JRIDE	100.00%	91.66%
Sequential	85.41%	83.33%
JE-MAP	56.25%	47.25%

Table 3: Material identification performance for JRIDE versus alternative algorithms.

The main focus of our Year 6 work was transitioning some of the multispectral algorithms developed in earlier years for use in commercial CT systems for DHS missions. We focused on developing algorithms for a dual-energy air cargo CT inspection system developed by our industrial partner, Astrophysics Inc. The specific prototype system we focused on is known as the Multi-View CT (MVCT) Cargo System. The system is designed as a noninvasive inspection method for the screening and detection of contraband and explosives in cargo skids at ports of entry. In 2017, the system was demonstrated in government trials using some of the single-energy reconstruction algorithms developed in our earlier work. The system has been deployed at J.F.K. International Airport in New York [44]. However, the current algorithms need improved processing to reduce imaging artifacts due to effects of beam hardening, photon starvation, and noise. In addition, the system reconstructs each spectrum independently, leading to a fundamental loss in resolution.

To enhance the resolution of the resulting dual-energy system, we developed a major improvement for the joint inversion approach SPDE that we had developed earlier in our program, described earlier. This approach, EPTV regularization, is described in our paper [31]. Figure 9 shows the differences between the standard FBP reconstruction, the SPDE reconstruction, and our new EPTV reconstruction on two slices of a bag containing metal objects. As the figure indicates, the EPTV reconstructions do a better job of localizing the difficult reconstruction of photoelectric absorption when compared with the SPDE reconstruction. Both reconstructions are far superior to that obtained from filtered back-projection. Our EPTV algorithm can also be applied to single-spectrum reconstructions. We have done a prototype implementation for the Astrophysics MVCT instrument for single-spectrum reconstructions, and we are evaluating the enhancement in resolution in that limited-angle reconstruction scenario.

As the results in Figure 9 indicate, reconstructing photoelectric absorption is a challenging problem in the presence of metal because the majority of the low energy photons that carry the most information about photoelectric absorption fail to reach the detectors. In collaboration with Lawrence Livermore National Laboratory (LLNL), we have explored alternative approaches for basis decomposition that are more suitable

for higher energy systems and provide more stable features in the presence of metal. In particular, we have been using a synthetic monoenergetic basis decomposition which is derived from the photoelectric absorption and Compton scatter basis functions. Figure 10 shows the reconstruction obtained using the EPTV algorithm with the photoelectric and Compton basis functions, versus the synthetic monoenergetic basis (SMB) functions. As the figure indicates, the reconstructions with SMB basis functions at low energies are much more stable than the photoelectric reconstructions, as each of the basis functions can be estimated using the high-energy photons that are more likely to reach detectors in the presence of metal. A significant advantage of SMB features is that there are analytical methods for estimating the effective atomic number Z_{eff} and the electron density ρ_{eff}, which are features that allow for system-independent material characterization [27].

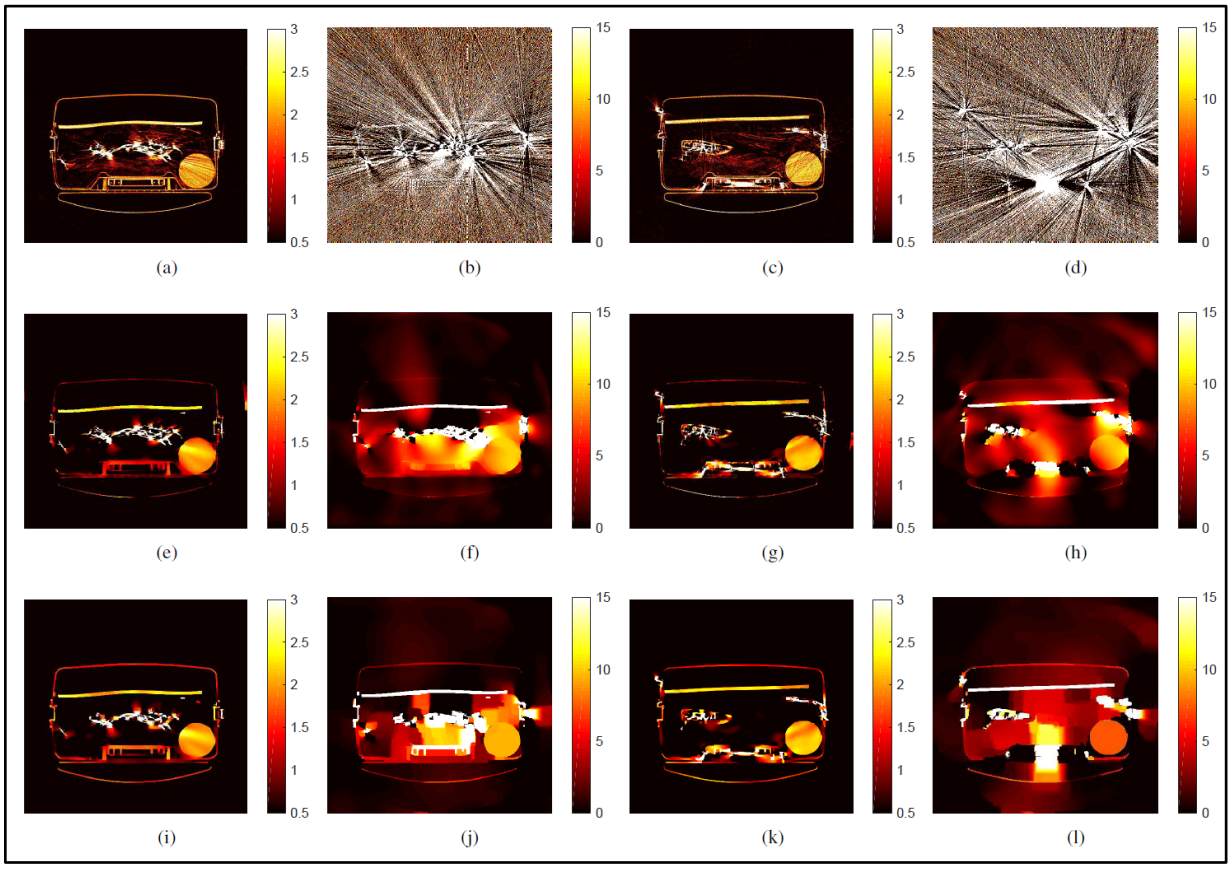

Figure 9: Reconstruction of two slices for container with metal. FBP reconstructions are shown with (a, c) Compton coefficients and (b, d) photoelectric coefficients. SPDE reconstructions are shown with (e, g) Compton coefficients and (f, h) photoelectric coefficients. EPTV reconstructions are shown with (i, k) Compton coefficients and (j, l) photoelectric coefficients.

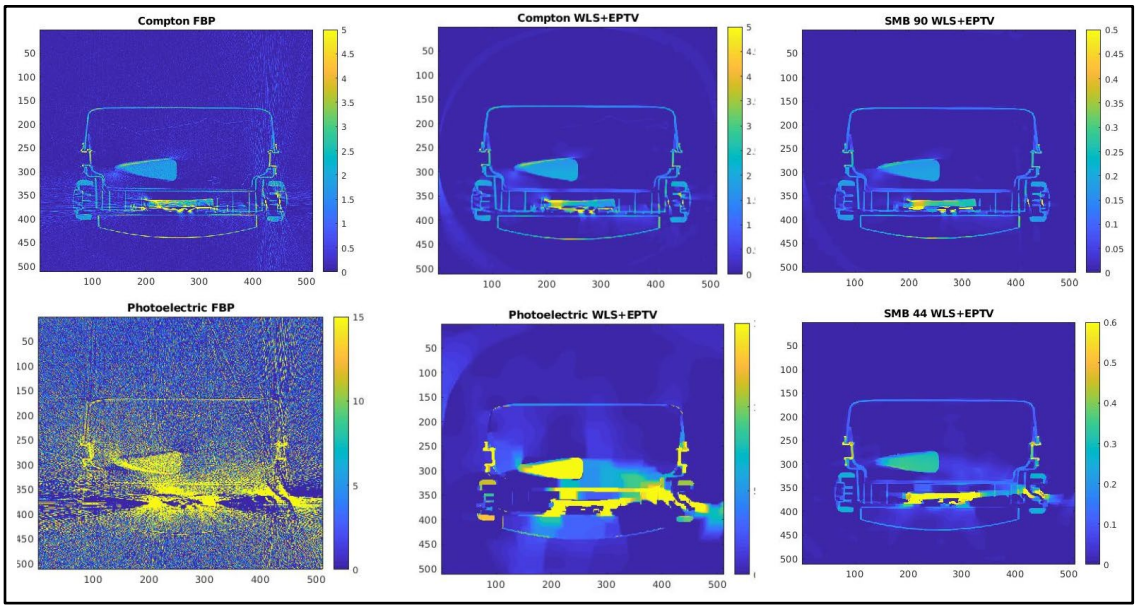

Figure 10: (left) FBP of Compton and photoelectric, (center) EPTV of Compton and photoelectric, and (right) SMB of high and low reconstructions.

In our final Year 7 work, the data-domain deep learning methods were extended to seamlessly include learned image models in a modular framework allowing for improved reconstruction even for very challenging problems. This new framework, called DIP-MIR, combines learned prior models for data and image using consensus equilibrium, as shown in Figure 11.

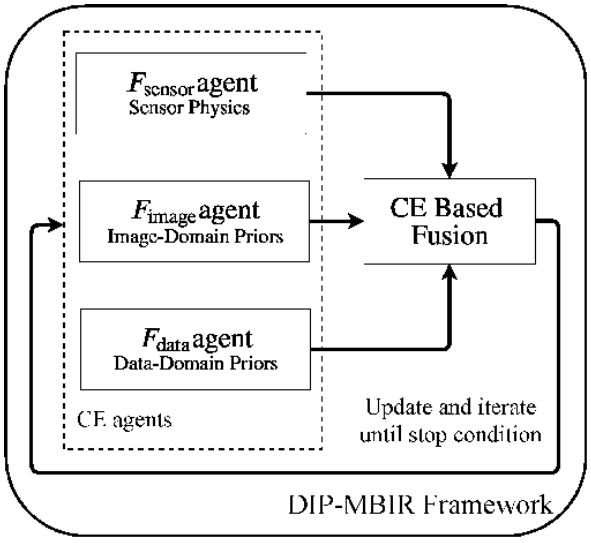

Figure 11: Consensus equilibrium-based framework for inclusion of deep learning of both data and image behavior.

Results from an extremely limited data reconstruction example using 90 degrees worth of data are shown in Figure 12, comparing a state-of-the-art deep network post-processing method to the new integrated approach.

Quantitative metrics in Table 4 confirm the visually apparent improvements provided by the new deep learning framework.

Method	RMSE	PSNR	SSIM
FBP + deep post-processing	103	23.32	0.48
PnP — MBIR existing model based	78	25.65	0.79
New DIP — MBIR deep learning based	51	29.50	0.87

Table 4: Reconstruction performance comparison of different methods in Figure 12.

In Year 7, we continued our transition work for dual-energy imaging with applications to cargo screening. A fundamental issue that arose in the transition effort is that material identification was that the presence of metal in cargo introduced significant artifacts that limited material recognition. We explored approaches for enhancing material recognition in the presence of metal artifacts. In our earlier work, we had developed techniques for compensating for metal artifacts that improved image quality. However, the improved quality often translated into erroneous material recognition, as the sonogram interpolation techniques modified the reconstruction parameters used for recognition.

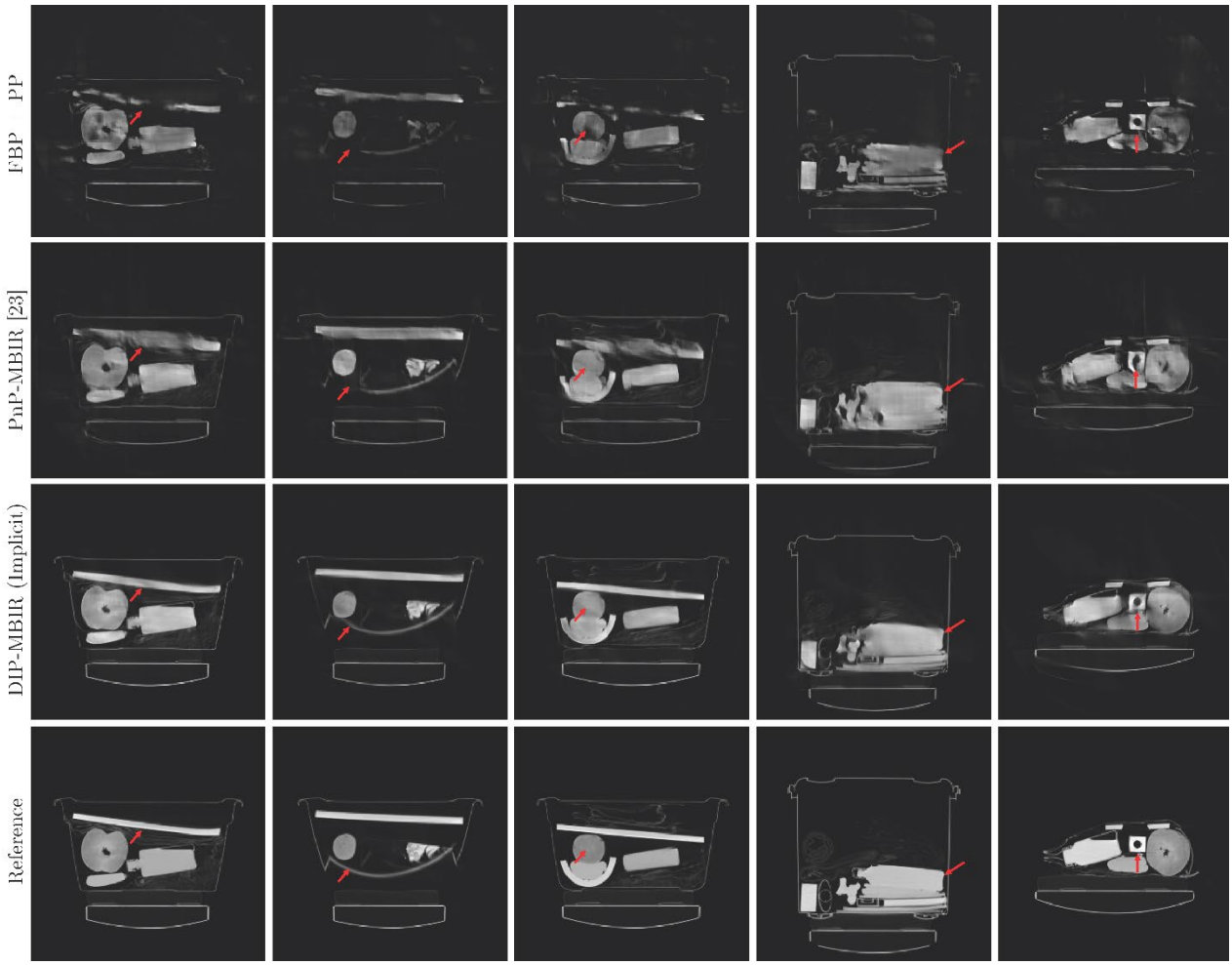

Figure 12: (top row) State-of-the-art deep-learning post-processing and (second row) model-based reconstruction compared to (third row) the new integrated consensus equilibrium-based deep-learning framework and (bottom row) ground truth for a challenging limited-angle tomographic reconstruction problem.

We conducted an in-depth study to determine whether the choice of basis functions in dual-energy reconstructions can mitigate the distortion in material recognition when metal is present. We explored the use of photoelectric and Compton basis (PCB) functions, synthesized monochromatic basis (SMB) functions, and material basis (MB) functions composed of polystyrene and aluminum for reconstruction. Using the reconstructed coefficient images, we generated estimates of effective atomic number and density. We simulated phantoms with regions of homogeneous materials between two copper sheets. The materials used in the simulations included a range of effective atomic number and electron density materials: polypropylene, citric acid, water, sapphire, magnesium, aluminum, black powder, hydrochloric acid, and, calcium chloride. For all cases, we conducted reconstructions using two different algorithms: total-variation (TV) and EPTV, with phantoms with and without metal present.

The results are shown in Table 5. The table depicts the averages of relative mean absolute errors for effective atomic number Z_e and electron density ρ_e across all materials. The results indicate two preliminary conclusions. First, reconstruction with EPTV results in enhanced accuracy for estimation of material properties for all three basis decompositions. The improvements were critical in the presence of metal, where the standard TV reconstruction techniques resulted in sizeable parameter errors, whereas the EPTV reconstructions led to much more accurate parameter estimates for all basis functions. The second conclusion is that material basis reconstructions may generate more robust material property estimates in the presence of metal. These preliminary conclusions require further experimentation with more complex phantoms for validation.

Mean error (%)	Directly from PCB		Sampled LAC from PCB		Sampled LAC from MB		Directly from SMB	
	Z_e	ρ_e	Z_e	ρ_e	Z_e	ρ_e	Z_e	ρ_e
TV (without metal)	0.71	0.75	0.72	0.55	0.99	0.86	0.72	0.65
EPTV (without metal)	0.43	0.56	0.42	0.18	0.98	0.74	0.41	0.24
TV (without metal)	49	2.7	49	33	52	66	40	29
EPTV (without metal)	11.8	1	11.7	0.8	2.4	3.9	5.4	4.8

Table 5: Average error in estimates of effective atomic number Z_e and electron density ρ_e across all materials, when imaged in the presence of metal and without metal.

The above results did not include any explicit sinogram correction to remove metal artifacts. Instead, they relied on the joint reconstruction algorithms to generate accurate coefficient images in the regions of interest. Most sinogram correction techniques have been developed for single energy spectrum systems and reduce artifacts such as metal blooming and streaking, as evidenced in our results in Figures 5 and 6. However, for material recognition, it is important to correct metal artifacts in multispectral images consistently and to estimate accurately the properties of the materials in the region. In Year 7, we conducted an investigation into developing dual-energy algorithms for material property estimation in the presence of metal. We explored approaches that apply dual-energy sinogram correction techniques for MAR prior to basis decompositions, as well as approaches that apply sinogram correction techniques after basis decomposition to the coefficient sinograms. We also explored algorithm variations to down-weight the accuracy of projections that include significant metal content. This is ongoing work that will be completed in the summer of 2020.

Our initial results [45] are shown in Table 6, for two phantoms with significant metal content and four materials of interest: water, nylon, citric acid, and aluminum. In these algorithms, we used both a PCB basis decomposition and a material basis decomposition using aluminum and polystyrene. The results are encouraging; we are able to estimate the effective atomic number and the electron density of materials within 1.5% of their true values using either of the two basis decompositions. Our goal this summer is to transition

these algorithms to work with cargo skids that contain boxes with some metal content, showing that we can generate accurate material property estimates.

Scatter v3	Effective Atomic Number		Effective Electron Density	
	Pho-Comp	Material	Pho-Comp	Material
Aluminum	0.07%	0.68%	0.19%	0.47%
Water	1.52%	2.10%	0.59%	0.80%
Citric Acid	0.53%	0.39%	0.23%	0.20%
Nylon	0.37%	0.46%	0.22%	0.15%
Average	0.62%	0.90%	0.31%	0.40%

Scatter v5	Effective Atomic Number		Effective Electron Density	
	Pho-Comp	Material	Pho-Comp	Material
Aluminum	0.00%	0.66%	0.05%	0.42%
Water	0.79%	0.35%	1.18%	1.74%
Citric Acid	1.88%	1.24%	3.63%	3.61%
Nylon	0.25%	0.32%	0.29%	0.29%
Average	0.73%	0.64%	1.29%	1.51%

Table 6: Average percent error in estimates of effective atomic number Z_e and electron density ρ_e across four materials, with two phantoms, when imaged in the presence of metal. The reconstruction algorithms use the EPTV algorithms with basis decompositions using either PCB or MB bases.

D. Milestones

Major milestones achieved to date include:

- Extended integrated segmentation and labeling framework from 2D to 3D.
- Developed and implemented performance prediction framework.
- Developed ADMM-based discrete tomography methods.
- Fused the artifact mitigation reconstruction and the integrated labeling frameworks into a discrete tomography framework, resulting in the JRIDE algorithm.
- Incorporated dictionary-based representations for multi-energy tomographic inversion and material characterization, resulting in the SPECK feature basis and associated reconstruction algorithms.
- Extended the SPDE framework to multi-energy sensing and from 2D to 3D using the SPECK basis.
- Developed and evaluated extensions of deep learning techniques for MAR in CT systems.
- Developed fast GPU versions of multi-energy CT algorithms for transition to cargo and checkpoint CT systems.
- Developed EPTV joint reconstruction for enhanced resolution.
- Developed multi-spectral CT reconstruction techniques using synthetic measurement bases.
- Transitioned reconstruction algorithms into a prototype MVCT cargo skid scanner, developed by Astrophysics Inc.
- Evaluated performance of multispectral CT algorithms with experimental data in collaboration with LLNL using multispectral micro-CT systems.
- Transitioned multispectral CT algorithms to LLNL through reports for potential integration into Livermore Tomography Tools.
- Developed and evaluated extensions of deep learning techniques for limited-angle CT reconstruction.
- Developed and evaluated new framework for inclusion of deep learning models of data and images for challenging data CT reconstruction problems.

- Developed fast, enhanced resolution versions of multispectral CT algorithms and transitioned to cargo CT systems.
- Evaluated performance of multispectral CT algorithms in prototype cargo system for material recognition.
- Developed approaches for multispectral CT material property recognition in the presence of significant metal content and transitioned them to cargo CT systems.

E. Final Results at Project Completion (Year 7)

This project developed methods to improve imagery for explosives detection and restricted object detection in X-ray-based sensing for checked luggage, checkpoints, and air cargo skids. Furthermore, it developed algorithm technology that takes advantage of new developments in sensor technology, which will enable future systems to address emerging threats, and integrated emerging concepts in machine learning. In Years 6 and 7, some of these reconstruction technologies were transitioned to a commercial cargo screening system. Over the life of the project, new algorithms and methods were developed that provided improvement over conventional methods of reconstruction for mono- and multi-energy X-ray CT scans. These algorithms provide the foundation for future CT systems that use multi-spectral excitation to obtain robust signatures for material identification.

III. RELEVANCE AND TRANSITION

A. Relevance of Research to the DHS Enterprise

The improved artifact suppression methods enhance image quality, object boundary and volume estimates, and object localization. The direct discrete inversion approaches make better use of existing measurements, allowing for better detection. The multispectral CT algorithms can provide enhanced information for discriminating complex, higher effective atomic number explosives better than conventional dual-energy systems, increasing the probability of detection and resulting in fewer false alarms for both checkpoint and checked-luggage systems. The deep learning-based inversion frameworks allow for greatly improved imagery for challenging imaging problems. The multispectral material property reconstruction algorithms that work robustly in the presence of metal provide the foundation for automated threat recognition algorithms that can work in difficult luggage and cargo screening scenarios.

Overall, these methods can increase the probability of detection as well as reduce the number of false alarms, which can, in turn, reduce the need for on-screen anomaly resolution protocol (OSARP) and manual inspection. These concerns will grow as the use of multi-spectral X-ray scanning increases at the checkpoint.

B. Status of Transition at Project End

The most significant transition of this work has been in collaboration with Astrophysics Inc., where we have transitioned subsets of the developed algorithms to a fielded air cargo skid scanner. Algorithms transitioned include several dual-energy reconstruction algorithms for limited angle CT, including edge preserving regularization as well as enhanced material property reconstruction algorithms in the presence of metal for improved automated threat recognition. While several algorithms have been transitioned, additional modifications are in progress as our partner Astrophysics Inc. adds operational requirements for their instrument.

C. Transition Pathway and Future Opportunities

In developing next-generation reconstruction algorithms, we have engaged in extensive discussions with potential transition partners. However, upgrading software in certified instruments is seldom desirable unless there are new requirements that the instrument must satisfy. Hence, we focused our attention on vendors developing new instruments. Our industrial partner, Astrophysics Inc., was developing a novel limited-field-of-view, dual-energy CT scanner for cargo skids and needed algorithms that significantly extended the state of the art for this design. We focused much of our transition work on this direction, and our algorithms have been at the heart of the CT reconstruction used in Astrophysics's Multi-View CT Cargo Scanner. We have continued our discussions with other vendors, looking for new opportunities for transitioning our algorithms.

D. Customer Connections

- Francois Zayek, Astrophysics Inc., ALERT industrial partner, met weekly.
- Harry Martz and Kyle Champley, LLNL, met twice per month.
- Ronald Krauss and Robert Kleug, DHS, met occasionally.

IV. PROJECT ACCOMPLISHMENTS AND DOCUMENTATION

A. Education and Workforce Development Activities

1. Student Internship, Job, and/or Research Opportunities
    a. Ms. Devadithya will be an intern at Lawrence Livermore National Laboratory in the Materials Research Institute working under Dr. Harry Martz. Her internship was delayed until Sept. 2020 because of Livermore workplace restrictions due to the COVID-19 virus.

B. Peer Reviewed Journal Articles

1. Ghani, M.U., & Karl, W.C. "Fast Enhanced CT Metal Artifact Reduction Using Data Domain Deep Learning." *IEEE Transactions on Computational Imaging*, *6*, 27 August 2019, pp. 181–193. https://doi.org/10.1109/TCI.2019.2937221.

Pending –

1. Ghani, M.U., & Karl, W.C. "Integration of Data and Image Priors for Image Reconstruction Using Consensus Equilibrium." Submitted to *IEEE Transactions on Computational Imaging.*

C. Peer Reviewed Conference Proceedings

1. Ghani, M.U., & Karl, W.C. "Integrating Data and Image Domain Deep Learning for Limited Angle Tomography Using Consensus Equilibrium." *IEEE Conference on Computer Vision*, Seoul, Korea. 22 October–2 November 2019.
2. Ghani, M.U., & Karl, W.C. "Integrating Learned Data and Image Models through Consensus Equilibrium," in *Computational Imaging*, Bouman, C.A., & Sauer, K., editors, *Process of Electronic Imaging*, Burlingame, CA. 26–30 January 2020.
3. Ghani, M.U., & Karl, W.C. "Integrating Learned Data and Image Models through Consensus Equilibrium for Model-Based Image Reconstruction." *International Symposium on Biomedical Imaging*, Iowa, IA. April 2020.

4. Devadithya, S., & Castañón, D. "Material Identification in Presence of Metal for Baggage Screening," in *Computational Imaging*, Bouman, C.A., & Sauer, K., editors, *Process of Electronic Imaging*, Burlingame, CA. 26–30 January 2020.

D. Other Presentations

1. Karl, W.C. "Data and Image Domain Deep Learning for Tomographic Computational Imaging." Invited talk in *Institute for Mathematics and its Applications Workshop on Computational Imaging*, 14–18 October 2019.

E. Student Theses or Dissertations Produced from This Project prior to Year 7

1. Chen, K. "Reconstruction Algorithms for Multispectral Diffraction Imaging." PhD Thesis, electrical engineering, Boston University, May 2014.
2. Eger, L. "Enhanced Information Extraction in Multi-Energy X-Ray Tomography for Security." PhD Thesis, electrical engineering, Boston University, May 2014.
3. Tuysuzoglu, A. "Robust Inversion and Detection Techniques for Improved Imaging Performance." PhD Thesis, electrical engineering, Boston University, May 2014.
4. Babaheidarian, P. "Algorithms for Enhanced Artifact Reduction and Material Recognition in Computed Tomography." PhD Thesis, electrical engineering, Boston University, May 2018.
5. Sun, Z. "Reduced and Coded Sensing Methods for X-Ray Based Security." PhD Thesis, electrical engineering, Boston University, September 2016.

Pending –

1. Ghani, M.U. "Data and Image Domain Deep Learning for Tomographic Computational Imaging." PhD Thesis, electrical engineering, Boston University, in progress—expected completion December 2020.
2. Devadithya, S. "Enhanced Reconstruction and Material Recognition in X-Ray CT for Security Applications." PhD Thesis, electrical engineering, Boston University, in progress—expected completion May 2021.

V. REFERENCES

[1] R. E. Alvarez and A. Macovski, "Energy-selective reconstruction in X-ray computerized tomography," *Physics in Medicine & Biology, vol. 21, no. 5,* 11976, pp. 733–744.

[2] A. C. Kak and M. Slaney, "Principles of Computerized Tomographic Imaging," Society of Industrial and Applied Mathematics, 2001.

[3] J. A. Fessler, I. A. Elbakri, P. Sukovic, and N. H. Clinthorne, "Maximum-likelihood dual-energy tomographic image reconstruction," Proc. of SPIE, *vol. 4684*, 2002, pp. 38–49.

[4] K. W. Dolan, R. W. Ryon, D. J. Schneberk, H. E. Martz, and R. D. Rikard, "Explosives detection limitations using dual-energy radiography and computed tomography," Proceedings of the First International Symposium on Explosives Detection Technology, 1991, pp. 252–260.

[5] S. Singh and M. Singh, "Explosives detection systems (EDS) for aviation security," *Signal Processing 83*, 2003, pp. 31–55.

[6] J. Heismann, J. Leppert, and K. Stierstorfer, "Density and atomic number measurements with spectral X-ray attenuation method," *Journal of Applied Physics* 94, 2073-9, 2003.

[7] B. De Man, J. Nuyts, P. Dupont, G. Marchal, and P. Suetens, "Metal streak artifacts in X-ray computed tomography: a simulation study," *IEEE Transactions on Nuclear Science, V. 46*, June 1999, pp. 691–696.

[8] Z. Ying, R. Naidu, and C. R. Crawford, "Dual energy computed tomography for explosive detection," *Journal of X-ray Science and Technology, vol. 14, no. 4*, 2006, pp. 235–256

[9] A. Macovski, *Medical Imaging Systems*, Prentice-Hall, 1983.

[10] L. Martin, A. Tuysuzoglu, W. C. Karl, and P. Ishwar, "Learning-based object identification and segmentation using dual-energy CT images for security," *IEEE Transactions on Image Processing, vol. 24*, *no. 11*, 2015.

[11] L. Martin, W. C. Karl, and P. Ishwar, "Structure-preserving Dual-energy CT for Luggage Screening," Proc. of IEEE International Conference on Acoustics, Speech, and Signal Processing, Florence, Italy, 4–9 May 2014.

[12] L. Martin, "Enhanced Information Extraction in Multi-Energy X-ray Tomography for Security," Ph. D. Thesis, Electrical Engineering, Boston University, May 2014.

[13] Y. Boykov, O. Veksler, and R. Zabih, "Fast approximate energy minimization via graph cuts," *IEEE Transactions Pattern Analysis Machine Intelligence*, *vol. 23, no. 11*, 2001, pp. 1222–1239.

[14] P. Babaheidarian and D. A. Castañón, "Joint Segmentation and Material Recognition in Dual-Energy CT Images," Proc. 2017 IS&T International Symposium on Electronic Imaging, San Francisco, CA, 29 January–2 February 2017.

[15] P. Babaheidarian, "Algorithms for Enhanced Artifact Reduction and Material Recognition in Computed Tomography," Department of Electrical and Computer Engineering, Boston University, January 2018.

[16] A. Tuysuzoglu, W. C. Karl, I. Stojanovic, D. A. Castañón, and S. Unlu, "Graph-Cut Based Discrete-Valued Image Reconstruction," *IEEE Transactions on Image Processing, vol. 24, no. 5*, pp. 1614-1627, 2015.

[17] A. Tuysuzoglu, "Robust Inversion and Detection Techniques for Improved Imaging Performance," Doctoral Thesis, BU, ECE Department, June 2014.

[18] S. Boyd, N. Parikh, E. Chu, B. Peleato, and J. Eckstein, "Distributed optimization and statistical learning via the alternating direction method of multipliers," *Foundation and Trends Machine Learning*, *vol. 3, no. 1*, January 2011, pp. 1–122.

[19] A. Tuysuzoglu, Y. Khoo, and W. C. Karl. "Variable Splitting Techniques for Discrete Tomography," Proceedings of IEEE International Conference on Image Processing, Phoenix, Arizona, 25–28 September 2016.

[20] A. Tuysuzoglu, Y. Khoo, and W. Clem Karl, "Fast and robust discrete computational imaging," in *Computational Imaging*, C. A. Bouman, K. Sauer, editors, Proc. of Electronic Imaging, San Francisco, CA, 29 January – 2 February 2017.

[21] A. Tuysuzoglu, Y. Khoo, W. Clem Karl, and U. Ghani, "Fast and Robust Discrete Computational Imaging," in International Conference on Computational Photography, Stanford University, Stanford, CA, 12–14 May 2017.

[22] Y. Zhang, H. Yan, X. Jia, J. Yang, S. Jiang, and X. Mou, "A hybrid metal artifact reduction algorithm for X-ray CT," *Medical Physics, V. 40*, 2013.

[23] W. A. Kalender, R. Hebel, and J. Ebersberger, "Reduction of CT artifacts caused by metallic implants," *Radiology, vol. 164, no. 2*, 1987.

[24] F. E. Boas and D. Fleischmann, "Evaluation of two iterative techniques for reducing metal artifacts in computed tomography," *Radiology, vol. 259, no. 3*, 2011.

[25] S. Ravishankar and Y. Bresler, "Learning sparsifying transforms," *IEEE Transactions on Signal Processing, V. 61, No. 5*, 2013.

[26] P. Babaheidarian and D. A. Castañón, "A Randomized Approach to Reduce Metal Artifacts in X-Ray Computed Tomography," Proceedings of IS&T International Symposium on Electronic Imaging, San Francisco, CA, 29 January – 2 February 2017.

[27] S. G. Azevedo, H. E. Martz, Jr., M. B. Aufderheide, III, W. D. Brown, K. M. Champley, J. S. Kallman, G. P. Roberson, D. Schneberk, I. M. Seetho, and J. A. Smith, "System-independent characterization of materials using dual-energy computed tomography," *IEEE Transactions on Nuclear Science, V. 63*, February 2016

[28] V. Berisha, A. Wisler, A. O. Hero, III, and A. Spanias, "Empirically estimable classification bounds based on a nonparametric divergence measure," *IEEE Transactions on Signal Processing, V. 64*, February 2016.

[29] T. Montgomery, W. C. Karl, and D. A. Castañón, "Performance Estimation for Threat Detection in CT Systems," *Proc. of SPIE, vol. 10187*, SPIE, Los Angeles, CA, 9–13 April 2017.

[30] P. Babaheidarian and D. A. Castañón, "Feature Selection for Material Identification in Spectral CT,"in Computational Imaging, C. A. Bouman, K. Sauer, editors, Proc. of Electronic Imaging, San Francisco, CA, 28 January – 2 February 2018.

[31] S. Devadithya and D. Castañón, "Edge-preserving Total Variation Regularization for Dual-Energy CT Images," IS&T Symposium on Electronic Imaging, San Francisco, CA, January 2019.

[32] C. R. Crawford, "Research and Development of Reconstruction Advances in CT-Based Object Detection Systems," ALERT TO3 final report, May 2014.

[33] P. Luc, Pauline. C. Couprie, S. Chintala, and J. Verbeek, "Semantic Segmentation using Adversarial Networks." NIPS Workshop on Adversarial Training, Barcelona, Spain, December 2016.

[34] M. U. Ghani and W. C. Karl, "Deep learning based sinogram correction for metal artifacts reduction," in Computational Imaging, C. A. Bouman, K. Sauer, editors, *Proc. of Electronic Imaging*, San Francisco, CA, 28 January – 2 February 2018.

[35] M. U. Ghani and W. C. Karl, "CNN based Sinogram Denoising for Low-Dose CT," in Imaging and Applied Optics 2017 (3D, AIO, COSI, IS, MATH, pcAOP), OSA Technical Digest, Optical Society of America, Orlando, FL, 25–28 June 2018.

[36] M. U. Ghani and W. C. Karl, "Learning based methods for CT correction," in International Conference on Computational Photography 2018, Carnegie Mellon University, Pittsburgh, PA, 4 – 6 May 2018

[37] M. U. Ghani and W. C. Karl, "Sinogram Inpainting using Deep Learning," 2018 IEEE Image, Video, and Multidimensional Signal Processing (IVMSP) Workshop, Zagori, Aristi Village Greece, 10–12 June 2018.

[38] M. U. Ghani and W. C. Karl, "Deep learning in artifact reduction for medical imaging," Gordon Research Conference: Creating Knowledge from Imaging Data, Easton, MA, 17–22 June 2018.

[39] N. G. Anderson, A. P. Butler, et al., "Spectroscopic (multi-energy) VT distinguishes iodine and barium contrast material in mice," *European Radiology, vol. 20, no. 9*, 2010.

[40] Q. Yang, W. Cong, Y. Xi, and G. Wang, "Spectral X-ray CT image reconstruction with a combination of energy-integrating and photon-counting detectors," *PLoS One, vol. 11, no. 5,* 2016.

[41] S. Feuerlein, E. Roessl, R. Proksa, G. Martens, O. Klass, M. Jeltsch, V. Rasche, H. Brambs, M. Hoffmann, and J. Schlomka, "Multienergy photon-counting K-edge imaging: potential for improved luminal depiction in vascular imaging," *Radiology, vol. 249, no. 3*, 2008, pp. 1010–1016.

[42] P. Babaheidarian and D. A. Castañón, "Joint reconstruction and material classification in spectral CT," Proc. of SPIE: Anomaly Detection and Imaging with X-Rays (ADIX) III, SPIE Defense + Security, Orlando, FL, April 2018.

[43] K. Nakada, K. Taguchi, G. S. Fung, and K. Amaya, "Joint estimation of tissue types and linear attenuation coefficients for photon-counting CT," Medical physics 42(9), pp. 5329–5341, 2015.

[44] F. Zayek, "The Multi-View CT Air Cargo Pallet Scanner," ADSA 21 presentation, Northeastern University, November 2019. 2018.

[45] S. Devadithya and D. Castañón, "Material Identification in Presence of Metal for Baggage Screening," IS&T Symposium on Electronic Imaging, San Francisco, CA, January 2020.